JOINT EUROPEAN TORUS JET

JET–P(85)15

R.J. Bickerton
et al

Latest Results from JET

Latest Results from JET

R.J. Bickerton, F. Alladio[1], D.V. Bartlett, K. Behringer, R. Behrisch[2], E. Bertolini, C. Best, T. Bonicelli, G. Brjcco[1], M. Brtisati, D.J. Campbell, P.G. Carolan[3], J. Christiansen, P. Chuilon, J.P. Coad, J.G: Cordey, S. Corti, A.E. Costley, F. Crisanti[1], C. deMichelis, B. Denne, K.J. Dietz, D.F. Düchs, P.A. Duperrex[5], A. Edwards, S. Ejima[6], W.W. Engelhardt, J. Ehrenber[2], S.K. Ererit[3], B.T. Ericksson, M.J. Forrest[3], M.G deberg[7], A. Gibson, R. Gill, A. Gondhalekar, D. Goodall[3], N. Gottardi, C. Gowers, B.J. Green, G. Grosso[8], N.C. Hawkes[3], J. Hemmerich, F. Hendricks[9], M. Huart, M. Huguet, J. Jacquinot, O.N. Jarvis, E.M. Jones, E. Kallne, J.C. Kallne, A. Xellman [6], S Kissel, L. de Kook, H. Krause[2], H. Kukral[2], P. Lallia, J. Last, E. Lazzaro, P. Lomas, G. McCracken[3], G. Magyar, M. Malacarne, M. Mansfield, V. Marchese, P. Martinel1i[2], F.K.Mast[2], P.L. Mondino, P.D. Morgan, A.W. Morris[3], G. Murphy, M.F.F. Nave, P. Nielsen, R:M. Niestadt[10], P. Noll, J. O'Rourke, D. Pasini[11], N.J. Peacock[3], H.W. Piekaar[10], A. Pochelon[5], R. Prentice, P.H. Rebut, D.C. Robinson[3], R. Ross, G. Sadler, A. Santaguistina, F.C. Schueller; S. Segre[1], M.F: Stamp, P: Stangeby[12], C.A. Steed, P.E. Stott, T.E. Stringer, D. Summers, H.P. Summers, J.A. Tagle[13], A. Tanga, A Taroni, P.R. Thomas, K. Thomsen[9], G. Tonetti[5], B.J.D: Tubbing[10], M: ·Turner[3], M. Valisa[9], P. van Belle, H. van der Beken, M.L. Watkins, J. Wesson, and V. Zanza[1]

JET-Joint Undertaking, Culham Science Centre, OX14 3DB, Abingdon, UK

[1]*EURATOM-ENEA Association, Frascati, Italy*
[2]*EURATOM-IPP Ass.ociation, Iflstitut fUr Plasmaphysik, Garching, Federal Republic of Germany*
[3]*EURATOM-UKAEA Association, Culham Laboratory, Abingdon, UK*
[4]*EURATOM-CEA Association, Fontenaj aux Roses, France*
[5]*EURATOM-Suisse Association, CRPP CH-1007, Lausanne, Switzerland*
[6]*G.A. Technologies, P.O. Box 85608, San Diego, Ca., USA*
[7]*EURATOM-Danish Association, Ris6, Denmark.*
[8]*EURATOM-CNR Association, Institute di Fisica del Plasma, Milan, Italy*
[9]*EURATOM Fellow*
[10]*EURATOM-FOM Association, Rynhuizen, The Netherlands*
[11]*University-of British Columbia, Vancouver, Canada*
[12]*Permanent address, Aerospace Institute, University of Toronto, Canada*
[13]*UNESA-ASINEL, Spain*

Preprint of Invited Paper presented to the 12th European Conference on Controlled Fusion and Plasma Physics, Budapest, Hungary, 2–6 September 1985

ABSTRACT.

In the last year, JET tokamak performance has been progress!vely raised, culminating in operation at the full design level of 5MA plasma current in a toroidal field at 3.4T. Plasma control has been improved with the plasma current, position, shape and line-average electron density all now controlled by feed-back systems. By glow discharge cleaning in hydrogen/methane mixtures, the interior of the vessel has been coated with carbon (carbonisation). This reduces the fraction of power radiatedto 50% and raises the density limit for disruption by 10%. Operation over a wide range of parameters, including varying major and minor radii, has given data for more extensive scaling studies. With ohmic heating, the maximum global energy confinement time is $0.8 \pm 0.$ls and the maximum central ion-temperature ~3.0keV. The highest ($\hat{n}\,\hat{\tau}_E\,\hat{T}_1$) product is reached with onmic heating in a deuterium plasma and is ~$6 \times 10^{19} m^{-3}$ s keV±20%.

KEYWORDS

Thermonuclear Fusion Research; Tokamaks; Joint European Torus; Plasma Diagnostics, plasma.

INTRODUCTION

The main parameters of the Joint European Torus (JET) are shown in Table 1. Typical pulse durations are 15s with current flat-top times of 5s or greater. The aims of the last year of ohmic operation have been to extend the operating range to the full design values, to get cleaner plasmas than hitherto and to establish a wider data base for scaling studies. All these aims have been achieved to some extent. Details of the JET apparatus and earlier results have been given by Rebut and Green (1984) and Rebut et al (1985).

TABLE 1 JET Parameters

Parameter	Design Value	Operational Values
Plasma minor radius (hor)	1.25m	0.8 - 1.2m
Plasma minor radius (vert)	2.10m	0.8 - 2.1m
Plasma major radius (R)	3.0m	2.5 - 3.4m
Toroidal magnetic field at R=3.0m	≤3.45T	≤3.45T
Plasma current (I_p)	≤4.8MA	≤5.0MA

TABLE 2 JET Carbonisation History

Glow discharge voltage 400V: Gas Pressure ~ 5.10^{-3}mbar

Date (number of Sessions)	Gas Mixture	Discharge Current (A)	Wall Temp (°C)	Duration (hours)
Aug 84 (2)	H_2-3%CH_4	3	250	1
Sept 84 (1)	H_2-3%CH_4	3	250	6
Jan 85 (1)	D_2-2%CH_4	5	300	6
Feb 85 (2)	D_2-2%CH_4	5	300	8
Mar-May 85 (5)	D_2-12%CH_4	5	300	6
Late May 85 (1)	D_2-17%CH_4	6	300	48

MACHINE OPERATION

Figures 1(a) and (b) show toroidal and poloidal cross-sections of the JET device. During 1985, the machine operated with 4 carbon limiters, 4 nickel limiters and 2 RF antennae

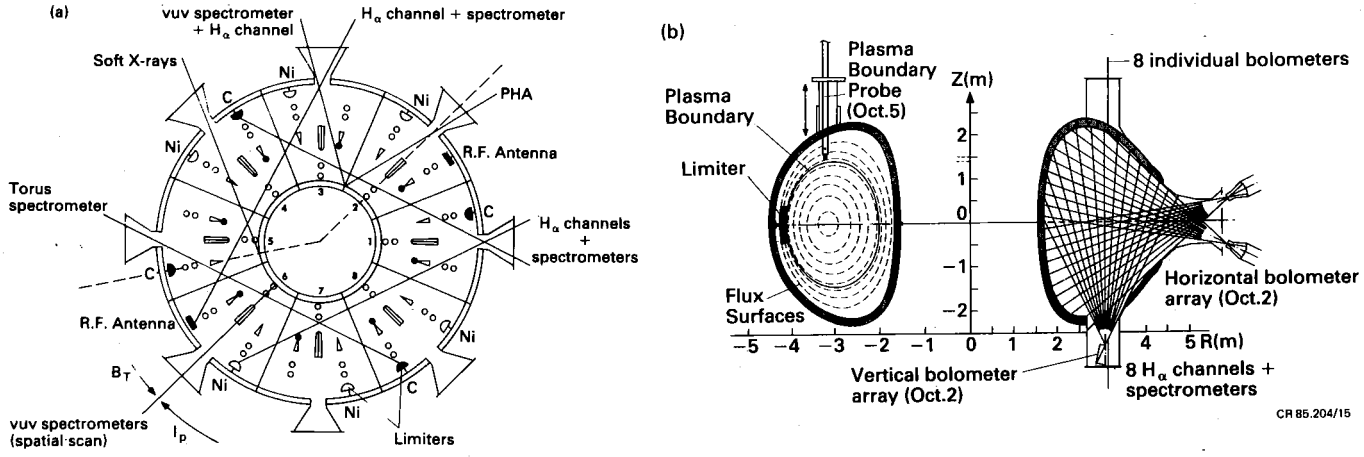

Fig. 1. (a) Toroidal and (b) Poloidal cross-section of the JET machine, showing the line-of-sight of various diagnostics. In (b), the left-hand poloidal cross-section is taken through Octant No. 5 (marked as the dotted line in (a)); and the right-hand poloidal cross-section is taken through Octant No.2 (shown as the dotted line in (a));

installed on the outer equatorial plane. The carbon limiters were the effective ones with the nickel limiters withdrawn 4cm behind. The antennae were also 2cm behind the carbon limiters for most of the operation. In addition the small major radius side of the interior of the vacuum vessel was covered to a height of ± 1m by carbon tiles for the 1985 operations. Figure 2 shows the vessel interior where all these features can be seen. The interior vessel wall was maintained at a temperature of about 300°C for all the experiments reported here. The base pressure was typically 10^{-7}mbar, comprising 10^{-7}mbar of hydrogen and 10^{-9}mbar of residual impurities. The vessel was conditioned by glow discharge cleaning in hydrogen, deuterium/methane or hydrogen/methane mixtures.

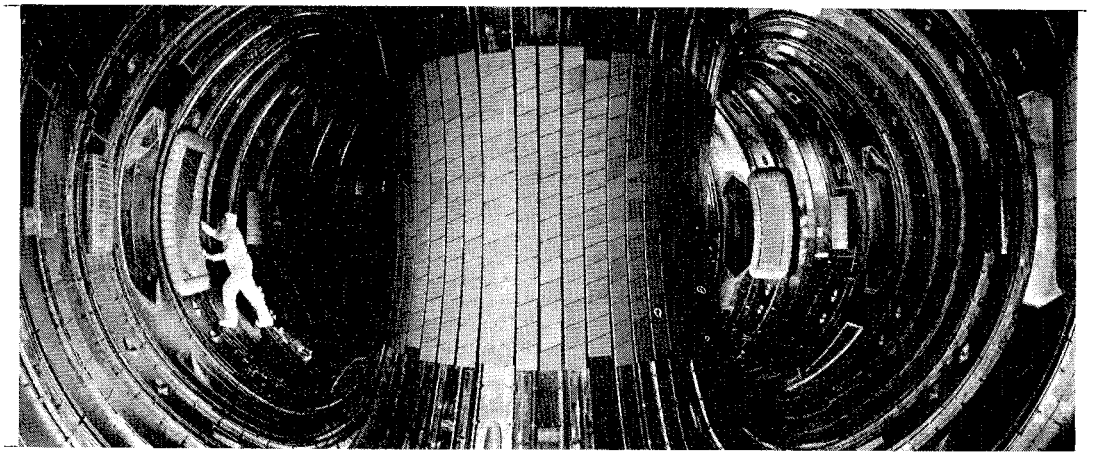

Fig. 2. Photograph inside the JET machine, showing the relative orientation of the two RF antennae, and the nickel and carbon limiters. The extent of the carbon protection tiles on the inner wall is also shown;

DIAGNOSTICS

a) The torus is equipped with 18 poloidal field pick-up coils inside each octant, continuous loops around the symmetry axis and local flux loops on the exterior surface of the vacuum vessel, enabling determination of plasma current, loop voltage, plasma boundary and the internal flux surfaces.

b) The electron temperature $T_e(r)$ profile is measured by an absolutely calibrated electron cyclotron emission (ECE) system viewing along several major radius chords in and close to the mid-plane. Michelson and Fabry-Perot interferometers and an echelon grating polychrometer are used to give varying frequency coverage and time resolution. The electron temperature is also measured by a single point Thomson scattering system, at a fixed point on the equatorial plane at a frequency of ~1Hz throughout the pulse. The 'fixed' point can be changed between pulses. Generally good agreement is obtained between the two methods (Costley et al 1985).

c) The electron density $n_e(r)$ is measured by a single channel 2mm microwave interferometer, and a seven channel far infra-red laser (190μm) interferometer system.

d) The ion temperature T_i is measured by a mass-selecting neutral particle analyser viewing the plasma along a chord in the mid-plane (Corti et al., 1985). In deuterium the ion temperature is also deduced from the neutron yield and from the energy distribution of the emitted neutrons with a ^{3}He spectrometer (Jarvis et al., 1985).

e) The effective ion charge Z_{eff} is deduced from the bremsstrahlung continuum intensity at 523nm viewed along a vertical chord. The electron temperature and density profiles from other diagnostics are used in the analysis.

f) The radiated power is measured by bolometers viewing along 34 chords at one poloidal location and by single bolometers in each octant. Assuming constant emissivity on magnetic surfaces, the multiple chord data is Abel inverted to give local radiated power densities (Gottardi et al., 1985).

g) The temperature and power flux in the scrape-off plasma have been measured with a single Langmuir/bolometer probe inserted from the top of the vacuum vessel (Stangeby et al., 1985).

h) Soft X-ray measurements have been made with diodes viewing the plasma horizontally on the mid-plane through various filter thicknesses. There is also a single chord pulse-height analyser system which gives a measure of metal ion concentrations (K-lines) and a secondary measurement of electron temperature (continuum).
i) Visible spectroscopic observations (viewing the plasma through ~100m of optical fibres) yield data on H_α emission and the influx of light impurities from the limiters and the walls. Two close-coupled spectrometers cover the ranges 200-700nm and 10-170nm yielding information on impurity species and ion states from which the central impurity concentrations can be deduced (Denne et al, 1985, Stamp et al, 1985).
j) Surface probes can be introduced into the torus to determine the nature of machine surfaces after glow-discharge cleaning and/or plasma operation (Coad et al., 1985). Long term samples, distributed over the interior vacuum vessel, are analysed after each experimental period.
k) An infra-red camera system (sensitive around 900nm) observes the emission from a carbon limiter. In some cases, this emission reflects the rise in surface temperature up to ~1500°C. In other cases, the temporal behaviour of the emission is not consistent with a temperature rise but may be due to emission from carbon lines or excited molecules. The two cases can be clearly distinguished.

PLASMA CONTROL

The plasma current time dependence is determined by a combination of pre-programming and feedback control of the excitation of the flywheel generator in the poloidal field circuit. The plasma density is also feedback controlled by varying the gas introduction rate according to the line density measured by the 2mm microwave interferometer. Since density can only be added in a controlled way, the system is ineffective when the gas release rate from wall and limiters is too high or is increased uncontrollably. Examples are the density rise accompanying sudden increases in power input from RF heating or large gas releases from walls and limiters immediately after carbonisation.

The plasma position and shape is determined in real-time from the magnetic signals. The radial position is maintained by a feedback system controlling coil PF4 voltage (Fig. 3). Up-down plasma symmetry is maintained by a similar system driving differential currents in

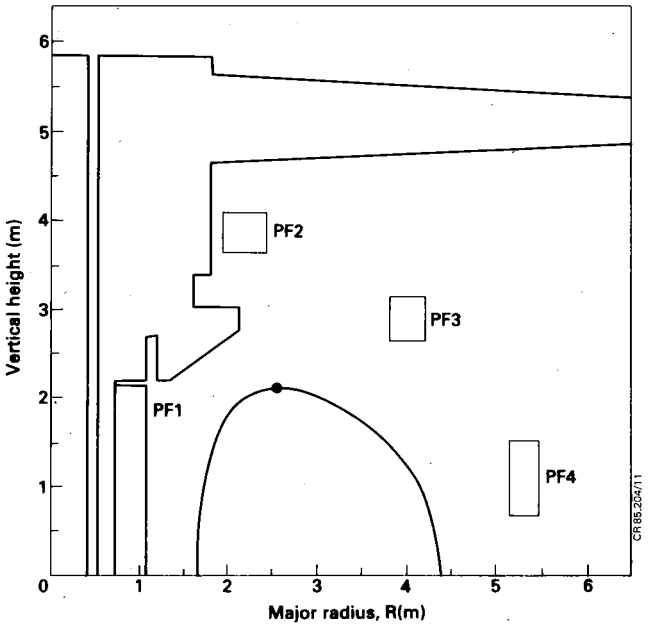

Fig. 3 Poloidal cross-section of JET machine showing relative positions of poloidal magnetic field coils 1,2,3 and 4;

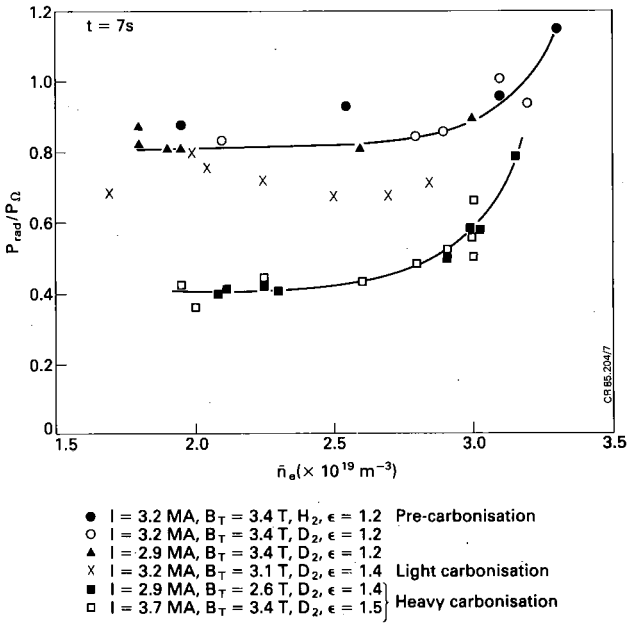

Fig. 4. Ratio of radiated power, P_{rad}, to ohmic input power, P_Ω, versus average electron density, $\bar{n}_e$, before and after carbonization;

sections of coils PF3 and PF4. The plasma shape is primarily determined by the proximity of plasma to the unsaturated parts of the iron magnetic circuit, ie by the plasma size, and by the magnitude of the quadrupole poloidal field generated by feedback - controlled opposite currents in the coils PF3 and PF4. With these feedback systems and under normal operating conditions, the flat-top current is held within 5% of the desired value, the radial position to ± 3cm, the vertical position to ± 1cm and the elongation ratio to within 5% of the pre-set value.

The initial "fast-rise" phase of JET operation is made by first charging the inductive store represented by the primary coil PF1 up to a pre-set current and then opening a switch across a resistor in the circuit. The higher the value of the resistor the higher the voltage applied at breakdown but also the faster the rate of plasma current rise in this phase. Experiments have shown excessive disruptive behaviour if the current rise rate exceeds ~1MA/s, probably due to skin currents and multi-valued q versus radius. To achieve adequate breakdown and a slow rise rate requires the charging current in PF1 coils to be limited to ~50% of its design value. Hence, only 25 of the theoretically available 34Vs can be used. For this reason, the record peak current of 5MA can be maintained at present only for about 1s. Modifications are planned to enable the resistor value to be reduced with time, giving a high breakdown voltage and a sufficiently slow current rise rate. Experiments on the breakdown phase are described in the papers (Thomas et al, and Schüller et al, 1985).

VERTICAL INSTABILITY

During one pulse in 1984, the growth rate of the vertical instability exceeded the capacity of the feedback system. The plasma current centre moved downwards 1m. without significant reduction in current (~2.6MA). Unexpectedly, very large forces (~300 tonnes) were transferred to the vacuum vessel causing significant displacements and a slight permanent distortion. The transfer of forces is now believed to be due to poloidal currents flowing radially through the plasma and returning in the rigid vessel sectors. Since then the vacuum vessel mounting has been considerably strengthened, with 16 tie-bars connecting the main ports to the iron limbs, restraining vertical motion and hydraulic dampers restraining the top and bottom vertical ports against sudden radial movements. Experiments with deliberately induced vertical instabilities at low currents have shown torus displacements reduced by a factor of ~3, when normalised to the square of the plasma current. Studies of these results and the growth rate dependence have lead to the imposition of an operating limit,

$$I_p^2 \, (b/a - 1.2) < 5.0 \; (MA^2) \qquad (1)$$

From this expression, it is clear that a current of 5MA cannnot be used with full plasma elongation (b/a~1.6). This limitation may be raised after further strengthening of the torus mounting and/or through a better understanding of vessel stresses. However, it seems likely that operation at currents of ~7MA will have to rely on a feed-back system with sufficient redundancy to protect the vacuum vessel from damage.

CARBONISATION AND IMPURITIES

"Carbonisation" of the torus interior is achieved by glow discharge cleaning in a mixture of hydrogen or deuterium and hydrogenic methane (CH_4). The carbonisation history of JET is shown in Table 2.

Analysis of samples exposed to carbonisation shows that carbon is diffused into the surface of inconel with a 100% coverage of the surface only being achieved in the case of the heavy carbonisation in 1985 ie. with 12% CH_4, 6 hrs or 17% CH_4, 48 hrs. (Coad et al., 1985).

Even before carbonisation, carbon was an important plasma impurity, due to the presence of carbon limiters and protection plates. The carbon concentration in the plasma core is

usually 2-3% n_e, and the limiters are the main source of carbon influx. Depending on the vacuum vessel cleanliness, 1-4%n_e of oxygen is found for which limiters and walls are both important sources. A few tenths of a percent of chlorine is believed to originate from torus washing after a vacuum opening. Concentrations of these light impurities are fairly insensitive to plasma currents and electron density. They increase in cases of stronger plasma-wall interaction, eg high elongations, and when approaching the density limit.

Nickel is the most important metal impurity. In addition, some chromium and iron are observed. Nickel and chromium are the main constituents of the Inconel vessel walls. The Faraday shields of the ICRH antennae present in the machine for 1985 operation are made of nickel. Metal impurities are especially prominent in low density plasmas. Their concentrations increase with plasma current, but decrease with plasma density, particularly steeply near the density limit for disruption.

During initial operation with new carbon tiles on the limiters, metal concentrations in the plasma were very low. After several weeks operation, the tiles become coated with metals probably due to strong plasma-wall interactions in disruptions. After some time, the metal deposit comes to an equilibrium level of ~10^{21} atoms/m^2, (found by surface analysis of limiter tiles after the 1983, 1984 and 1985 operation periods (Ehrenberg et al., 1985)). At this stage, the carbon limiters are the main sources of metal influx into the plasma. However due to the specific deposit topography, there is still about 90% carbon on the exposed surface.

After the initial contamination of the limiters, carbonisation was used routinely in 1985 to produce discharges with low metal content, and has been the most successful cleaning technique in JET so far. Before carbonisation JET plasmas had high radiation levels (70-100% P_Ω) and Z_{eff} was typically 4-5 or higher.

Carbonisation (first carried out in August 1984) led to an immediate reduction of metal concentrations and radiated power. Oxygen and chlorine reduced gradually after repetitive carbonisation to values below 1% and 0.05% respectively. After such repetitive carbonisation, P_{RAD} was only 40%P_Ω at moderate densities (ie the same value as with new limiter tiles) and 80%P_Ω at high density. The fraction of radiated power over input power versus electron density is shown in Fig. 4 (before and after a relatively light 1984 carbonisation). Z_{eff} was 3-4 for moderate and 2-3 for high electron densitites in the carbonised case.

Metal concentrations, derived from VUV spectroscopy, are about five times lower after a standard JET carbonisation (12% CH_4,6 hrs) but they recovered after some 20 plasma pulses to their previous level. A particularly heavy carbonisation carried out in 1985 (17% CH_4,48 hrs) resulted in a two orders of magnitude reduction in metals and a recovery time of ~200 plasma pulses. In 1984, the reduction in the fraction of power radiated for moderate densities lead to a clear heating of the limiter surface to 1800°C and metal was observed to evaporate from the surface. In 1985, even with low radiated fraction this heating has not been seen, presumably because of the proximity of relatively large antennae taking some of the load. The effect of the carbonisation on the Hugill diagram is shown in Fig. 5.

Carbonisation points are plotted indiscriminately without regard to the intensity used or the number of pulses after the treatment. However it can be seen that carbonisation extends the density limit by ~10%. Fig. 6 shows the radiated power profiles before and after carbonisation for similar plasma parameters. There is a reduction in the power radiated from the plasma core and a narrowing of the annular radiating zone surrounding the plasma.

Carbonisation is effective in reducing metal concentrations temporarily and oxygen on a longer timescale, but it leads to high carbon concentrations and thus a dilution of the working gas. For Z_{eff} ~3 and a carbon/oxygen ratio of 3:1, about 40% of the plasma electrons originate from impurities. Such depletion can be seen when comparing the neutron

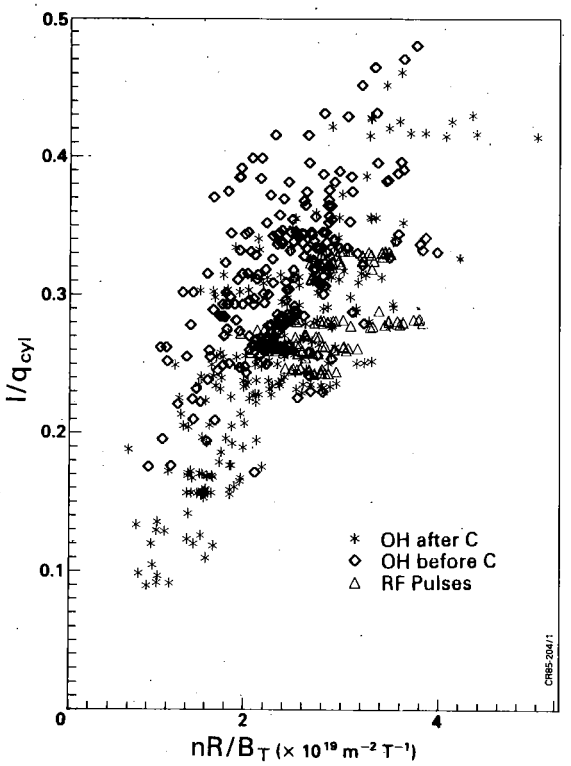

Fig. 5. Hugill-Murikami diagram of $1/q_{cyl}$ versus nR/B_T for ohmic plasma before and after carbonization and during R.F. heating.

yield with the ion temperature from the neutron spectrum. Agreement between the ion temperature deduced from the yield and that measured requires a deuteron/electron density ratio of typically 0.5 in the plasma core. Hydrogen release from the deposited carbon also makes density control difficult in the first few shots after carbonisation. However carbonisation is the only means found so far for reducing the radiated power once the limiters have become coated with metals.

Figure 7 shows Z_{eff} from bremsstrahlung measurements versus the ratio $\bar{n}_e/\bar{j}$ where $\bar{j}$ is the mean current density in the plasma, both before and after carbonisation. Carbonisation reduces Z_{eff} slightly but the minimum value is still high at ~2.5. To reduce this further, it is planned to surround the plasma more completely with low Z material, ie more carbon tiles. Other measures under discussion include gettering with beryllium or chromium and the use of beryllium limiter tiles.

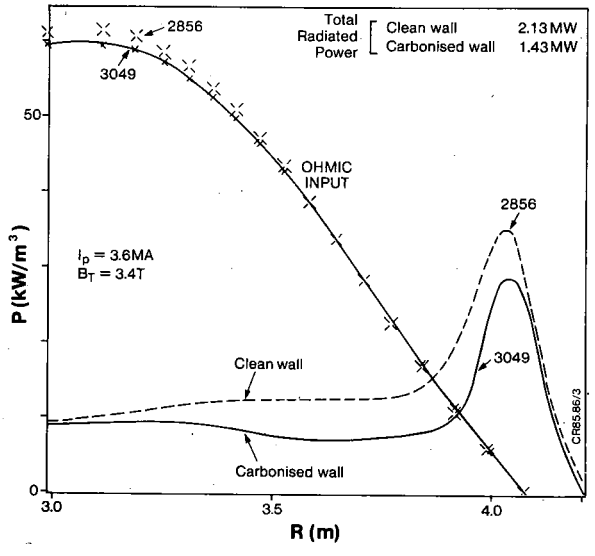

Fig. 6. Input ohmic power, P_Ω, and radiated power, P_{rad}, profiles for Pulse No: 2856 (before carbonization) and Pulse No: 3049 (after carbonization);

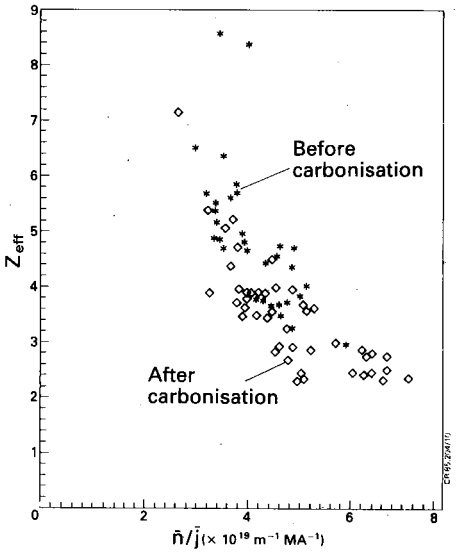

Fig. 7. The effective ion charge, Z_{eff}, from Bremsstrahlung measurements versus the ratio of average density, $\bar{n}$, to average current density, $\bar{j}$, both before and after carbonization;

EDGE PARAMETERS

Measurements of plasma parameters in the scrape-off layer of JET discharges have been performed in limited cases with an array of Langmuir and heat flux probes. An example is shown in Fig. 8 at I_p = 2.8MA, where the extrapolated plasma parameters at the plasma boundary are T_e ~100eV; n_e ~$2\times10^{18}m^{-3}$. The scrape-off layer profiles of $n_e(r)$ and $T_e(r)$, such as Fig. 8 (I_p ~2.8MA, $\bar{n}_e$ ~ $3\times10^{19}m^{-3}$, b/a~1.5,) have been used to calculate impurity generation rates due to sputtering of the limiter which are then compared with the spectroscopically observed influx. Only a small fraction of the impurity production at the limiters can be accounted for by hydrogen or deuterium impact. Under some conditions, the observed fluxes can be shown to be in rough agreement with carbon and oxygen ion sputtering.

The scrape-off layer $n_e(r)$ and $T_e(r)$ profiles were also used to calculate the shielding of the main plasma from impurities generated at the walls and limiters, and to compute the impurity content of the discharge. It is found that the scrape-off layer shields the main plasma quite effectively from impurities generated at the walls and that the principal, direct source of impurites in the core is due to the limiter. The values of n_e and T_e at the limiter tip are sufficiently high that all limiter impurities are ionised within a few centimetres of the limiter. The shielding of these limiter impurities is therefore approximately species-independent. The impurity density in the plasma can be estimated by balancing the impurity influx Γ_j particles from the limiters against the diffusive outflow,

$$\frac{n_j D}{\lambda_i+\lambda_{so}} = \frac{\Gamma_j}{A}$$

where n_j is the density of impurity species j in the plasma, λ_i the ionisation length for the impurity entering the plasma, λ_{so} the scrape-off layer thickness, D the diffusion coefficient for particles and A the plasma surface area. For JET, this gives $n_j \approx 10^{-3}\Gamma_j$ m^{-3}. Such concentrations are in agreement with measured values of Z_{eff} (~3) in such discharges.

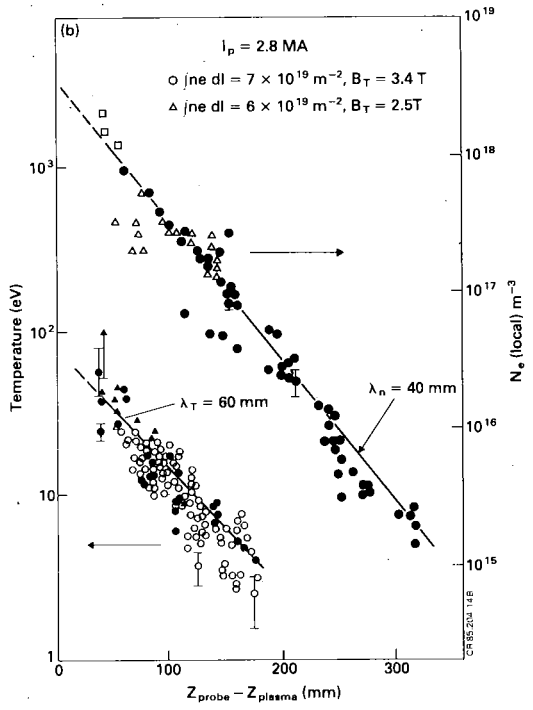

Fig. 8. Profiles of $T_e(z)$ and $n_e(z)$ for a standard I_p = 2.8MA discharge. All data was taken on the ion-side probes and during the discharge flat-top.

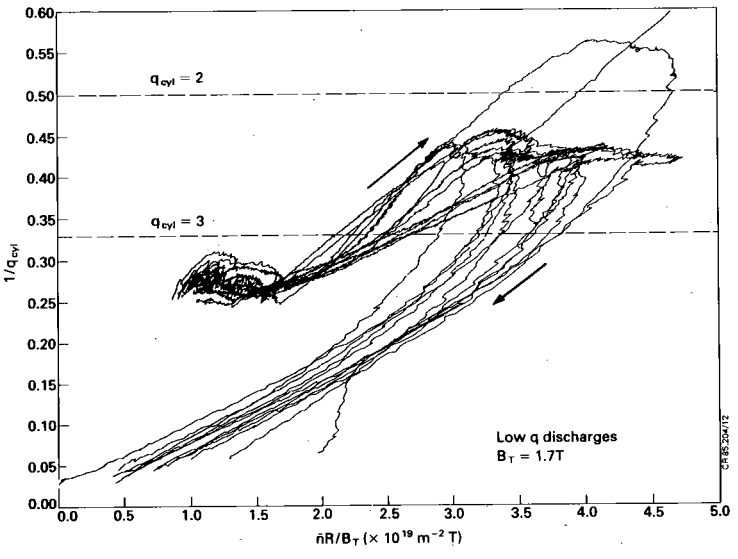

Fig. 9. Time trajectories in Hugill space ($1/q_{cyl}$ versus $\bar{n}R/B_T$) of low q discharges (B_T=1.7T) Current decay phase is lower bundle of trajectories;

Combining the H_α flux measured on the limiter and the power loading deduced from the surface temperature measurement at λ ~900nm reasonable agreement is obtained with the data from the Langmuir probe. The scrape-off layer thickness deduced from the thermal "footprint" on the limiter is in good agreement with the Langmuir probe measurements after correction for compression of the flux surfaces near the limiter on the mid-plane of the vessel.

Since the plasma-limiter contact dominates the influx of low and high Z impurites the limiter surfaces have been analysed by a variety of techniques and substantial coverage by (wall) metals was found after operations in 1983, 1984 and 1985. The surface concentration reflects broadly the plasma footprint on the limiter surface and the coverage is about 2.10^{21} atoms/m^2 for the colder edges down to 2.10^{20} atoms/m^2 in the hottest areas. Large ($\gtrsim$ 100μm: splashes) and small (~1μm) droplets are found in certain areas of the surface. On the limiter edges, an anomalously high concentration of D_2 (5.10^{21} atoms/m^2) was found and this is attributed to co-deposition of D_2 and carbon. The deuterium inventory in the limiters is ~10 times that in the plasma for one shot. Thus, the limiters represent a potential source for uncontrolled gas release if they become sufficiently hot.

DENSITY LIMITS

From the Hugill diagram (Fig. 5) it can be seen that the density limit (n_L) for ohmic discharges before carbonisation was

$$\bar{n}_L(m^{-3}) = 1.0\times10^{20}\ \frac{B(T)}{R(m)\ q_{cyl}}$$

and increases by about 10% after carbonisation. Although this is a small effect, there is a more important change from an operational point of view. Disruptions at the density limit after carbonisation tend to be slower and Marfe-like compared with hard disruptions before carbonisation.

At the density limit both before and after carbonisation, the contribution from metal impurities is small. The results are consistent with a model (Wesson et al, 1985) in which a density disruption occurs, whenever the radiated power from the annular zone outside the q_ψ=2 surface approaches 100%of the total input power. If the radiation is assumed to come from helium-like states of light impurities (Schüller et al, 1985, Gowers et al, 1985) then a fair agreement between experiment and observation is obtained. Since in this model $n_L\alpha(P/f)^{\frac{1}{2}}$ where P is the total input power and f the fractional impurity content, there should be no difficulty in raising the density limit by the required factor of 2 when the power input is increased from the present (ohmic) values of ~3MW up to a total of about 35MW. This assumes that, as in the present RF (< 5MW) experiments, f remains independent of P. Density limit disruptions may be of the Marfe (Stringer, 1985) type with strong initial poloidal asymmetries in the annular radiating layer or more conventional with approximate symmetry. (More details are given in O'Rourke, et al. 1985).

CURRENT LIMITS

With the density significantly less than the limiting density the discharge still disrupt in about 7% of cases over the whole data set. The probability of disruption peaks at ~20% for $3.2<q_{cyl}<3.5$. However, discharges have been made with q_{cyl} ~1.6 (q ~2.2) at 3.25MA in 1.7T field, without disruption. From this evidence, a 7MA discharge should be possible using the full aperture in JET. Concern about potential damage from disruptions or vertical instabilities precludes operation at this level for the present. Fig. 9 shows some of the trajectories in Hugill space of low q_{cyl} discharges. Note a common feature of tracking down the density limit line, as the discharge current and correspondingly $1/q_{cyl}$ fall at the end of the current pulse.

The time constant of the current quench phase depends whether the equilibrium field system can respond fast enough to maintain position control (Schüller et al., 1985). For currents <1MA, this control is maintained and the quench time is a constant 250ms. For currents >1MA, this becomes increasingly difficult and in the worst case the current fell from 3MA to zero in 10ms. In these "lost equilibrium" cases, the discharge moves rapidly to the small major radius side of the torus axis, interacting strongly with the inner wall. In such cases, the photoneutron production may reach 3.10^{14}/disruption with accompanying local photo-activation of the torus wall.

SAWTEETH

Sawteeth oscillations are seen on the signals from soft X-rays, neutrons, electron temperature, ion temperature and electron density in flat-top discharges for which q_{cyl} at the boundary is less than 12. Fig. 10 shows an example of sawteeth on the central electron temperature as measued by electron cyclotron emission. In many discharges, sawteeth are aperiodic and complex. In a simple case, the sawtooth period τ_{ST} is correlated with the global energy confinement time τ_E and for a particular data set the period of simple sawteeth scales as $\tau_{ST}/\tau_E = 0.13 \pm 30\%$. More commonly, in JET, the behaviour is dominated by giant sawteeth having roughly twice the period of the simple sawteeth (Campbell et al, 1985).

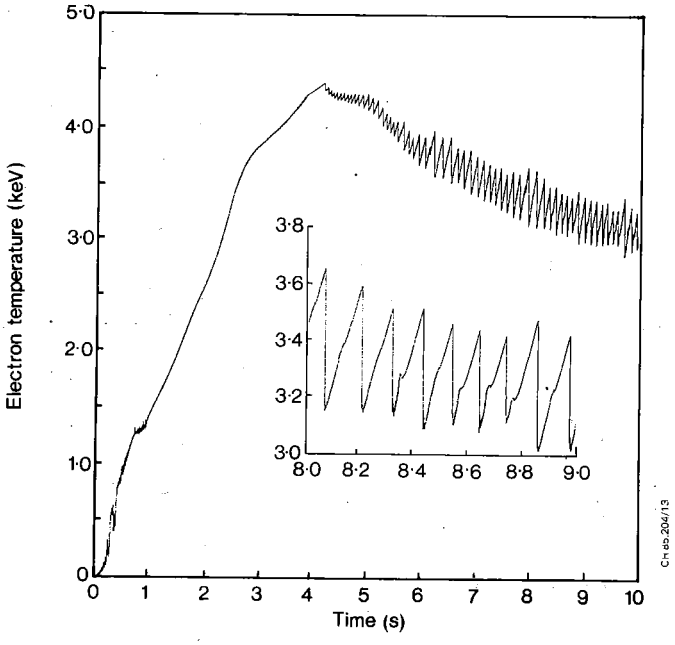

Fig.10. Central electron temperature, from ECE diagnostic, as a function of time (over 10s) showing sawtooth behaviour. The inset shows expended timescale (over 1s);

By using the fast electron cyclotron emission grating polychromator (Tubbing et al, 1985), it is possible to track the passage of the thermal wave excited by the sawtooth collapse in the plasma core. The observed propagation can be interpreted to give the effective electron thermal diffusivity $\bar{\chi}_{ep}$ and this can be compared with the value $\bar{\chi}_{eE}$ deduced from the global energy confinement time ($\bar{\chi}_{eE} = a^2/4.\tau_E$), typical results from a single shot during RF heating (1.3MW) and after RF during the Ohmic phase are

	$\bar{\chi}_{ep}$	$\bar{\chi}_{eE}$	$\bar{\chi}_{ep}/\bar{\chi}_{eE}$
RF	$3.5 m^2 s^{-1}$	$1.6 m^2 s^{-1}$	2.2
Ohmic	$3.4 m^2 s^{-1}$	$1.0 m^2 s^{-1}$	3.4

The reason for these differences is not known. A possible explanation is that the equilibrium profile is close to a state of marginal stability and any perturbation causes an enhancement in the thermal loss mechanisms. Another possibility is that there is an inward thermal pinch term analogous to that found for density diffusion.

HIGH CONFINEMENT AND HIGH CURRENT SHOTS

Figs. 11, 12 and 13 show a consistent set of data for a high confinement time shot. The discharge current is held at 3.6MA for a time of 6s. The minor radius is 1.2m and the elongation ratio b/a ~1.5. Towards the end of the current flat-top, the ohmic input power is 2.4MW and Z_{eff} ~2.6 (q_{cyl} ~ 3.5). Note the initial overshoot in central electron temperature which is not reflected in the volume average electron temperature. This is the consequence of the flattening with time of the electron temperature profile that can be seen in Fig. 13. Figure 14 shows the current wave-form for a 5MA shot. To minimise the chances of disruption these shots were run at intermediate density so that the corresponding global confinement time is not remarkable at ~0.5s. Nevertheless, these shots show the technical feasibility of full design performance in JET. Longer flat-top times will be feasible when, after circuit modification, the full volt-second capability can be used effectively.

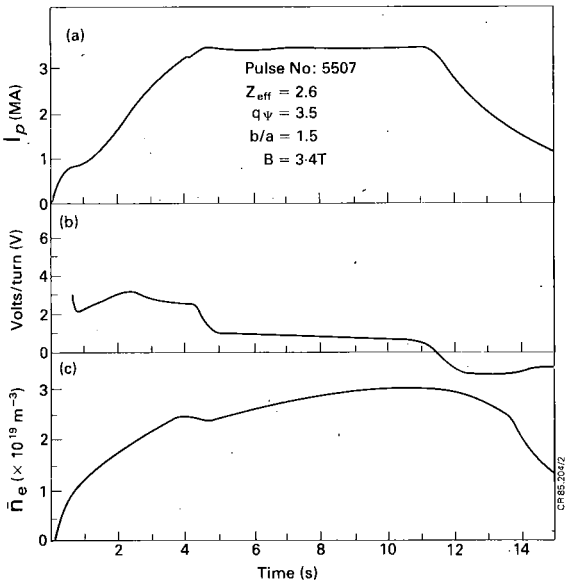

Fig.11. Pulse No:5507: (a) Current, (b) Volts per turn, and (c) Line average electron density versus time;

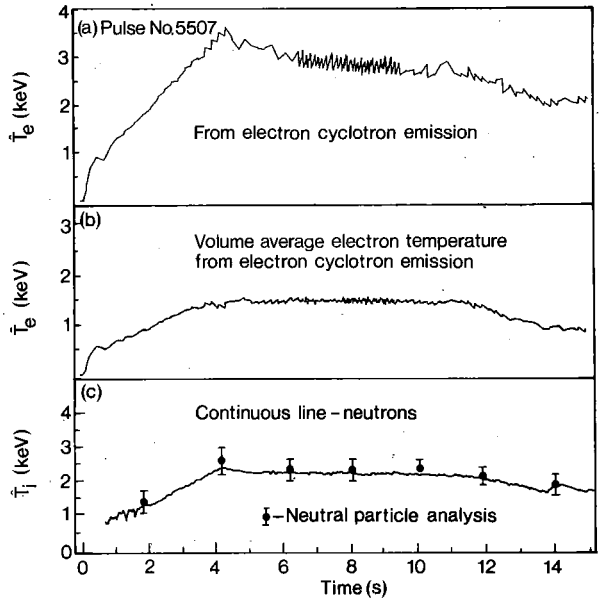

Fig.12. Pulse No:5507: (a) Peak electron temperature; (b) volume averaged electron temperature (from ECE); (c) Peak ion temperature versus time;

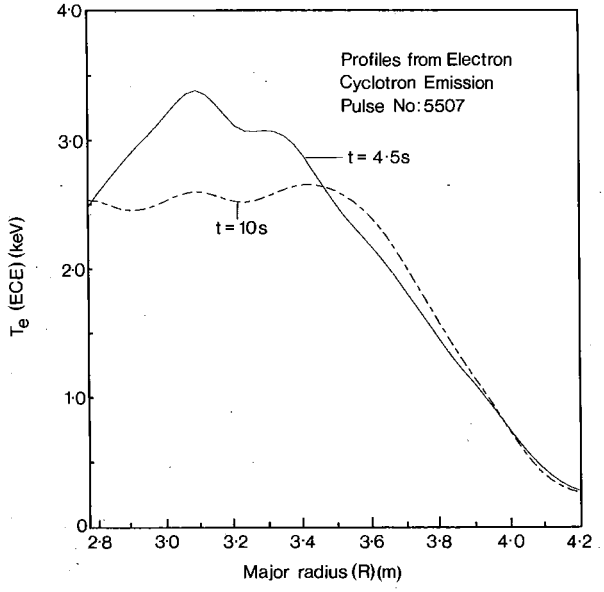

Fig.13. Electron temperature (T_e) profiles, from ECE measurements, at t=4.5s and t=10s in Pulse No:5507;

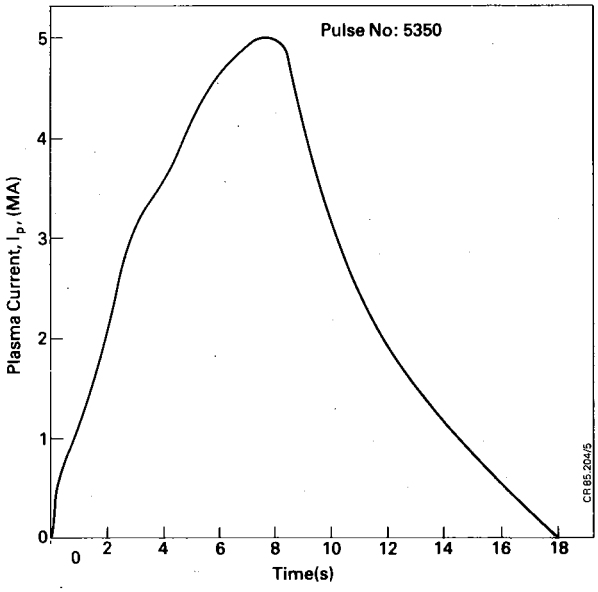

Fig.14. Plasma Current versus time for Pulse No:5350 showing achievement of 5MA plasma current;

CONFINEMENT TIME AND LAWSON PARAMETERS

The global confinement time (τ_E) is calculated near the end of the current flat-top when quantities are in an equilibrium state. τ_E is defined by $\tau_E=(W_e+W_i)/P_{input}$, where W_e and W_i are the electron and ion energy contents in the plasma. W_e is calculated simply using the known electron density and temperature profiles integrated over the volume of the derived magnetic surface. The ion energy content is calculated using the measured (NPA) central ion temperature, assuming that the radial profile has the same form as the electron temperature together with the ion density (n_i) from,

$$\frac{n_i}{n_e} = \frac{n_D}{n_e}^{(1+\gamma)} + \frac{n_o}{n_e} + \frac{n_c}{n_e}$$

(n_D, n_o and n_c are the deuteron, oxygen and carbon ion densities, respectively)

n_D/n_e is derived from the neutron yield using the neutral particle analyser ion temperature, γ is the ratio of hydrogen to deuterium (normally 5%) and the ratio n_o/n_c is calculated from the spectroscopic data. Together with the equation for charge neutrality

$$n_D + n_o\, 8 + n_c\, 6 = n_e$$

this determines n_i/n_e

The global confinement data for discharges in JET is plotted versus the scaling $R^2a\bar{n}q_{cyl}$ in Fig. 15. This is not the best regression fit to JET data but is shown here for comparison with earlier results from JET and TFTR. The best regression fit now shows a weaker dependence on density than found previously (J G Cordey et al, 1985). This may reflect the greater variation with density of the fraction of power radiated (Fig. 4) since the first carbonisation in late 1984.

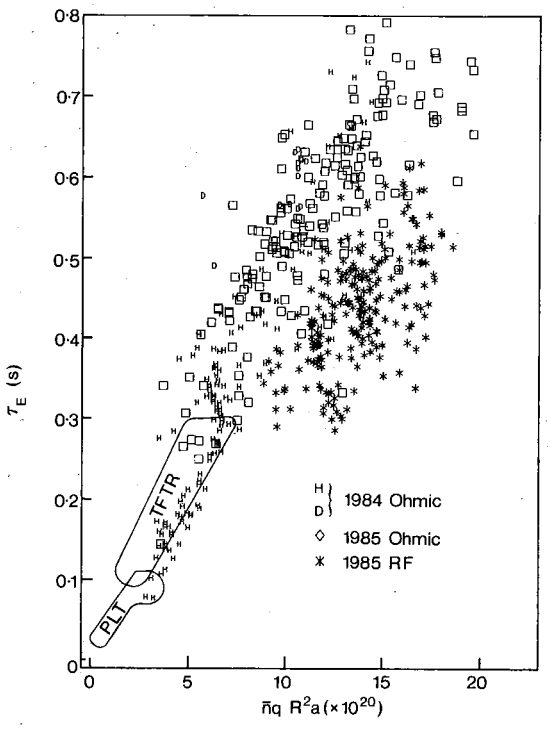

Fig.15. Global energy confinement time, τ_E, versus the scaling factor $\bar{n}qR^2a$ for both Ohmic and RF heated plasmas. The data from PLT and TFTR are shown for comparison;

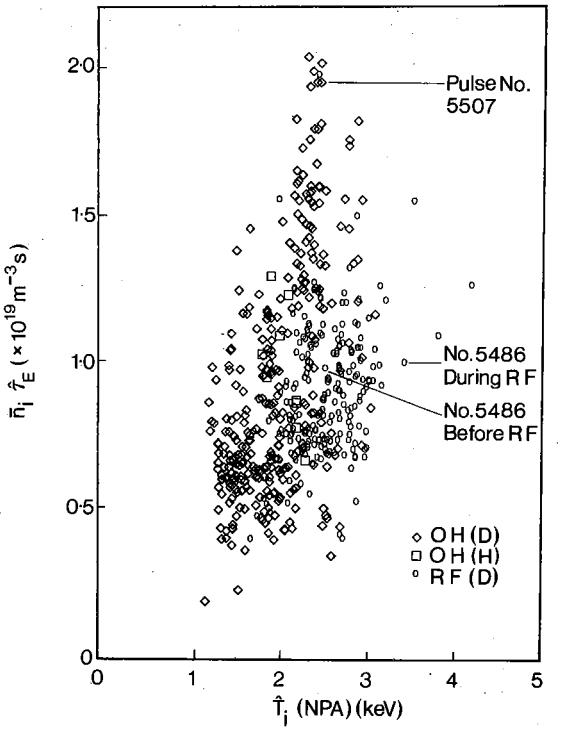

Fig.16. Lawson diagram of $\hat{n}_i\hat{\tau}_E$ versus $\hat{T}_i$(NPA) for both hydrogen(H) and deuterium(D) plasmas during ohmic and RF Heating. Pulse No:5507 and Pulse No:5486 (both before and during RF heating) are highlighted;

In Fig. 16 the performance of JET is plotted in the Lawson plane of $\hat{n}_i\hat{\tau}_E$ versus $\hat{T}_i$. Here n_i is the central hydrogen isotope density (usually significantly less than the electron density). τ_E is the central energy confinement time and T_i the central ion temperature. For a limited number of shots $\tau_E(\Psi)$ has been calculated where

$$\tau_E(\psi) = \frac{3/2 \int_0^{\Psi} n_e T_e + n_i T_i)\, dV}{P_\Psi}$$

P_Ψ is the power input inside the flux surface Ψ. P_Ψ is calculated from the known loop voltage and the current distribution deduced from magnetic measurements. $\tau_E(\Psi)$ is found to have a broad maximum inside the plasma half-radius, such that $\tau_E(\Psi) \sim 1.3\ \tau_E$ where τ_E is the global confinement time defined earlier. This ratio has then been applied to all the analysed shots on the Lawson diagram. The measured density profile generally has the form

$$n_e = \hat{n}\ (1 - r^2/a^2)^{\frac{1}{2}}$$

giving a ratio $\hat{n}/\bar{n}$ of $4/\pi$ where $\bar{n}$ is the line-average value.

The effect of RF heating in raising the central ion temperature can clearly be seen. The performance of ohmic heating plasmas is typically 20-40% higher in τ_E with deuterium rather than hydrogen plasmas, under similar conditions. With RF no attempt was made to increase the density above the Ohmic limiting value. In addition, RF was usually applied to standard ohmic plasmas with modest densities, ie discharges in which the ohmic confinement time was typically ~0.5s and not the highest attainable. Coupled with the observed degradation in τ_E when heating is applied, this leads to the RF discharges having the highest $\hat{T}_i$ but only modest $\hat{n}\,\hat{\tau}_E$. The highest value of the product $\hat{n}\,\hat{\tau}_E\,\hat{T}_i$ is ~6 $\times 10^{19} m^{-3} s$ keV, obtained with Ohmic heating. For the RF cases, τ_E is calculated assuming that all the power launched from the antennae is absorbed by the plasma. At present, power accounting is not accurate enough to prove this assumption.

MAGNETIC SEPARATRIX OPERATION

However, with this assumption, the first results with RF heating (Jacquinot et al, 1985) on JET show confinement time degradation similar to that seen on other machines with neutral beam or ion cyclotron resonance heating into limiter-bounded plasmas (Goldston 1984).

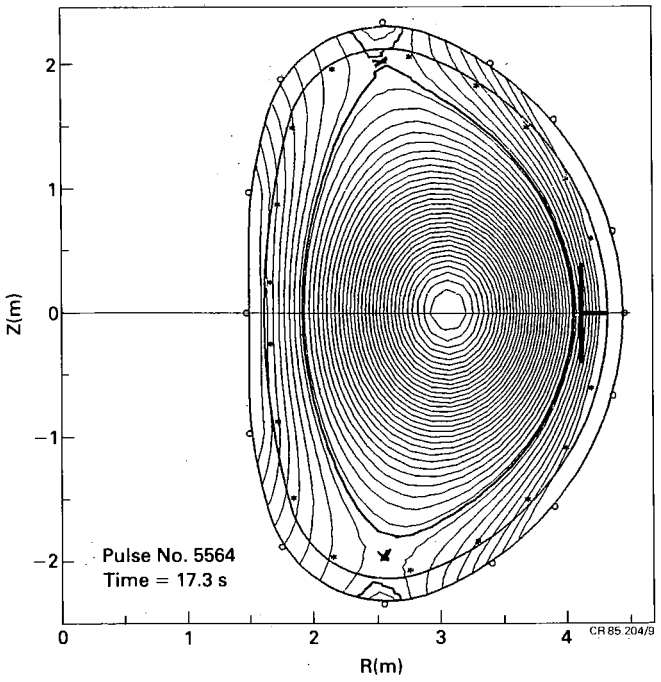

Fig.17. Pulse No:5564: (I_p=2MA, B_T=2.6T) showing formation of magnetic separatrices inside the vacuum vessel.

Starting with ASDEX, several tokamak devices (DIII,PDX) have shown that confinement can be greatly improved if the plasma is bounded by a magnetic separatrix. The JET poloidal field coil configuration allows the formation of a magnetic separatrix with two stagnation (or X-points) at the top and bottom of the vacuum vessel as an extreme case of plasma shaping. Experiments during Ohmic heating only have demonstrated this mode of operation and a number of technical questions relating to the up-down stability and the heat loads on the vessel have been studied (Tanga et al, 1985). Figure 17 shows the flux-contours for such a case at a current of 2MA in a field of 2.6T. The stable configuration was maintained by feed-back for several seconds. The corresponding plasma elongation is 1.7-1.8. In the region around the X-points, ~30% of the input power is radiated while interaction with the mid-plane limiters stops. The conduction/convection losses to the top and bottom of the vessel are estimated to be only 10-20% of the total power input. We believe that JET can be operated in this mode transiently for several seconds at a current level of 4MA without modification to the existing poloidal field coil system.

SUMMARY OF CONCLUSIONS

1) The electron density, plasma current, plasma position and shape are now controlled by feedback systems.
2) A 5 MA discharge has been achieved with a flat-top duration of ~1s. To extend this duration, the poloidal circuit will be modified to enable use of the full volt-seconds capability of the machine, consistent with breakdown and current rise-rate limitations.
3) The vessel supports have been strengthened so that performance at these higher levels was possible without risk of mechanical damage if vertical position control was lost. To go to full aperture plasmas at 5MA, further strengthening of the torus mounting will be required. To go to 7MA will require a feedback system with redundancy to minimise the risk of damage due to loss of position control.
4) Carbonising the vacuum vessel has both reduced Z_{eff} and given a modest increase in the critical density for disruption. However, the light impurities in the centre cause a considerable reduction (50%) in the ratio of deuteron to electron density. Immediately after carbonisation, breakdown and density control are difficult due to the release of retained hydrogen.
5) The observed density limits are consistent with the radiated power outside q=2 equalling the total input power at the limiting line in the $1/q_{cyl}$ vs $\bar{n}R/B$ plane. If this is the case, substantial increases in the density limit will be possible with full additional heating power, provided that the fractional impurity content does not increase with power.
6) JET has been operated down to q_{cyl}~ 1.6 (q_ψ = 2.2) at 3.25MA without disruption. On this basis, it should be possible to achieve 7MA in JET using full field and full aperture.
7) Sawtooth periods on JET are roughly linearly related to the global energy confinement time. Study of the heat pulse propagation shows an electron thermal diffusivity 2-4 times that deduced from the global energy confinement time.
8) By operating at full field, high aperture, and density near the limiting value, global energy confinement times of about 0.8s have been achieved with ohmic heating.
9) The highest central ion temperature of 4keV is achieved with RF heating. The best combination of Lawson parameters is obtained with ohmic heating, $\hat{n}\,\hat{\tau}_E = 2.2 \times 10^{19} m^{-3}s$ and $\hat{T}_i$ ~2.6keV, giving a product ($\hat{n}\,\hat{\tau}_E\,\hat{T}_i$) of ~$6 \times 10^{19} m^{-3}s$ keV.
10) Preliminary studies have demonstrated experimentally the ohmic operation of JET with a magnetic separatrix. This configuration when used with additional heating may permit an H-mode regime of confinement to be reached.

ACKNOWLEDGEMENTS

The authors wish to acknowledge the hard work and devotion of the many staff at all levels who built, modified and operated the machine for these experiments.

REFERENCES

Campbell,D.J., Bartlett,D.V., Best,C., Brusati,M., and coworkers. Proc. 12th European conference on Controlled Fusion and Plasma Physics (Budapest, Hungary, 1985). Vol 9F, Part 1, p. 130

Coad,J.P., McCracken,G.M., Erents,S.K., Ehrenberg,J., de Kock,L., Stangeby,P.C., Tagle,T. Proc. 12th European Conference on Controlled Fusion and Plasma Physics (Budapest, Hungary, 1985). Vol 9F, Part 2, p. 571

Cordey,J.G., Bartlett,D.V., Bickerton,R.J., Brusati,M., and coworkers. Proc. 12th European Conference on Controlled Fusion and Plasma Physics (Budapest, Hungary, 1985). Vol 9F, Part 1, p. 26

Corti,S., Bracco,G., Brusati,M., Gondhalekar,A., Grosso,G., Hendriks,F., Segre,S., Zanza,V. Proc. 12th European Conference on Controlled Fusion and Plasma Physics (Budapest, Hungary,1985). Vol 9F, Part 1, p. 219

Costley,A.E., Baker,E.A.M., Brusati,M., Bartlett,D.V., and coworkers. Proc. 12th European Conference on Controlled Fusion and Plasma Physics (Budapest, Hungary,1985). Vol 9F, Part 1, p. 227

Denne,B., Behringer,K.H., Engelhardt,W., Gill,R.D., and coworkers. Proc. 12th European Conference on Controlled Fusion and Plasma Physics (Budapest, Hungary, 1985). Vol 9F, Part 1, p. 379

Ehrenberg,J., Behrisch,R., Martinelli,P., Kukral,H., McCracken,G.M., Coad,J.P., de Kock,L. Proc. 12th European Conference on Controlled Fusion and Plasma Physics (Budapest, Hungary, 1985). Vol 9F, Part 2, p. 575

Goldston,R.J., (1984). Plasma Physics & Controlled Fusion, 26, 1A, 87

Gottardi,N., Krause,H., Mast,K.F. Proc. 12th European Conference on Controlled Fusion and Plasma Physics (Budapest, Hungary, 1985). Vol 9F, Part 1, p. 30.

Jacquinot,J., Anderson,R.J., Arbez,J., Bartlett,D., and coworkers. Special Issue of the Journal of Plasma Physics and Controlled Fusion. To be published

Jarvis,O.N., Gorini,G., Hone,M., Kallne,J., Merlo,V., Sadler,G., van Belle,P. Proc. 12th European Conference on Controlled Fusion and Plasma Physics (Budapest, Hungary, 1985). Vol 9F, Part 1,p. 223

O'Rourke,J., Campbell,D., Denne,B., Gondhalekar,A., and coworkers. Proc. 12th European Conference on Controlled Fusion and Plasma Physics (Budapest, Hungary, 1985). Vol 9F, Part 1,p. 155

Rebut,P-H., and Green,B.J. (1984). Plasma Physics and Controlled Fusion,26, 1A,1.

Rebut,P-H. et al., (1985). Plasma Physics and Controlled Nuclear Fusion, IAEA,(London) Vol.1,11.

Schueller,F.C., Alladio,F., Campbell,D., Crisanti,F., and coworkers. Proc. 12th European Conference on Controlled Fusion and Plasma Physics (Budapest, Hungary, 1985). Vol 9F, Part 1,p. 151

Schueller,F.C., Thomas,P.R., Kellman,a., Lazzaro,E., Lomas,P., Piekaar,H.W., Tanga,A. Proc. 12th European Conference on Controlled Fusion and Plasma Physics (Budapest, Hungary, 1985). Vol 9F, Part 1,p. 287

Stamp,M.F., Behringer,K.H., Forrest,M.J., Morgan,P.D., Summers,H.P. Proc. 12th European Conference on Controlled Fusion and Plasma Physics (Budapest, Hungary, 1985). Vol 9F, Part 2,p. 539

Stangeby,P.C., Erents,S.K., Tagle,J.A., McCracken,G.M., de Kock,L. Proc. 12th European Conference on Controlled Fusion and Plasma Physics (Budapest, Hungary, 1985). Vol 9F, Part 2, p. 579

Stringer,T.E. Proc. 12th European Conference on Controlled Fusion and Plasma Physics (Budapest, Hungary, 1985). Vol 9F, Part 1, p. 86

Tanga,A., Campbell,D.J., Denne,B., Gibson,A., and coworkers. Proc. 12th European Conference on Controlled Fusion and Plasma Physics (Budapest, Hungary, 1985). Vol 9F, Part 1, p. 70

Thomas,P.R., Christiansen,J.P., Ejima,S. Proc. 12th European Conference on Controlled Fusion and Plasma Physics (Budapest, Hungary, 1985). Vol 9F, Part 1,p. 283

Tubbing,B.J.D., Barbian,E., Campbell,D.J., Hugenholtz,C.A.J., Niestadt,R.M., Oyevaar,Th., Piekaar,H.W. Proc. 12th European Conference on Controlled Fusion and Plasma Physics (Budapest, Hungary, 1985). Vol 9F, Part 1,p. 215

Wesson,J., Gowers,C., Han,W., Mast,F., Nave,F., Turner,M., Watkins,M. Proc. 12th European Conference on Controlled Fusion and Plasma Physics (Budapest, Hungary, 1985). Vol 9F, Part 1,p. 147